Coupling mechanisms for optically induced NMR in GaAs quantum wells

Marcus Eickhoff, Björn Lenzman, Gregory Flinn,* and Dieter Suter
Universität Dortmund, Fachbereich Physik, 44221 Dortmund, Germany
(Received 21 May 2001; revised manuscript received 26 November 2001; published 13 February 2002)

Optical pumping can increase the polarization of nuclear spins in semiconductors such as GaAs by many orders of magnitude, improving the sensitivity in conventionally detected nuclear magnetic resonance (NMR) experiments. Optical detection of these NMR transitions provides an additional increase in sensitivity, and furthermore, can distinguish signal contributions from different quantum wells in multiple quantum well samples. In this article we study the coupling mechanisms for all-optical NMR experiments, where modulation of the cw optical excitation at the nuclear Larmor frequency induces transitions between the nuclear spin states. We find clear evidence for two different types of interaction between the photogenerated carriers and the nuclear spins: the hyperfine interaction and the coupling between the electric field of the electron and the nuclear quadrupole moment. While the former induces only $\Delta m_I = \pm 1$ transitions, the latter also causes (single photon-) $\Delta m_I = \pm 2$ transitions.

DOI: 10.1103/PhysRevB.65.125301 PACS number(s): 78.66.Fd, 76.70.Hb

I. INTRODUCTION

Nuclear magnetic resonance (NMR) investigations of nanometer-sized semiconductor structures, such as quantum films and quantum dots are not possible by standard radio-frequency (rf) detection techniques. However, it has been shown by various groups that optical pumping can increase the polarization of the nuclear spins by many orders of magnitude. As a result, rf detection of optically pumped GaAs quantum wells has been successfully reported in a slightly modified NMR probe.[1] It is also possible to detect the NMR transitions optically, through changes in the polarization of the photoluminescence.[2] While these experiments still utilized rf excitation of NMR transitions, it is also possible to replace the external rf field by a modulation of the optical field at the nuclear Larmor frequency. As a result, the NMR spectrum can be measured by purely optical means, eliminating the need for a rf coil.[3–7]

That it is possible to directly generate precessing magnetization by modulated optical excitation was demonstrated previously in atomic vapours,[8] using either mode-locked pulse lasers,[9,10] or cw lasers with external modulation.[11] In these experiments, the optical pumping directly creates transverse magnetization, which can accumulate over several Larmor periods if the modulation frequency matches the precession frequency.

When modulated laser beams are used to drive NMR transitions in semiconductors, the main effect is not a direct generation of precessing magnetization, but rather a reduction of the nuclear spin polarization when the resonance condition is fulfilled. In addition to the usual resonance condition $\omega_{\mathrm{mod}} = \gamma_n B_0$, it was also observed that optical excitation can induce transitions when the modulation frequency ω_{mod} becomes twice the Larmor frequency $\omega_{\mathrm{mod}} = 2\gamma_n B_0$. Kempf *et al.*[12] suggested that this effect could indicate that excitons can couple to nuclei through the electric quadrupole interaction.

An optimal excitation of NMR transitions by modulated optical pumping requires a strong hyperfine interaction with the photoexcited carriers. In typical bulk materials, this is achieved by trapping of the electrons in shallow donor sites.[2] In molecular beam epitaxy (MBE)-grown heterostructures, the donor density is too small to provide a sufficient number of trapping sites; instead, trapping typically occurs at interface defects.

II. SAMPLE DETAILS AND SETUP

Experiments were performed on a GaAs multiple quantum well sample. The quantum wells were grown by MBE on a (001) GaAs substrate. The well widths varied between 2.8 and 39.3 nm, and they were separated by 30.9 nm $Al_{0.3}Ga_{0.7}As$ barriers.

The sample was cooled to liquid helium temperatures in a He-flow cryostat. Excitation and detection were nearly resonant with the $n=1$ heavy hole transition of the 19.7 nm quantum well, whose photoemission peaks at 812.09 nm (width 0.44 nm; see Fig. 1). Excitation was on the high-energy side of the photoemission line and detection was on the low-energy side. The separation between excitation and detection (0.4 nm) was large enough to provide sufficient suppression of any scattered laser light.

A 100 mW laser diode was used for optical pumping as well as for the excitation of NMR transitions. The laser beam was either intensity or polarization modulated with an

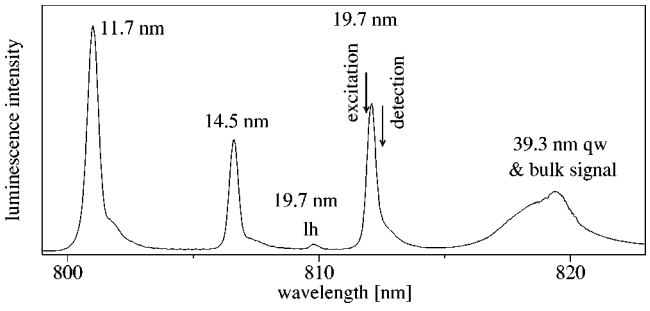

FIG. 1. Relevant section of the photoluminescence spectrum. The arrows mark the positions of excitation and detection. Well widths are indicated above the peaks. ''LH'' = light hole.

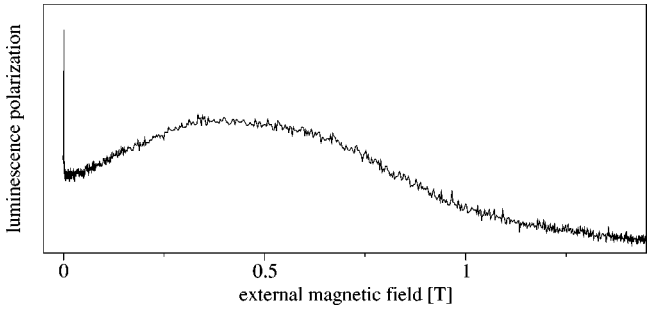

FIG. 2. Luminescence polarization as a function of the magnetic field (Hanle curve) measured after optical pumping in a field of $B_0 = 1.5$ T.

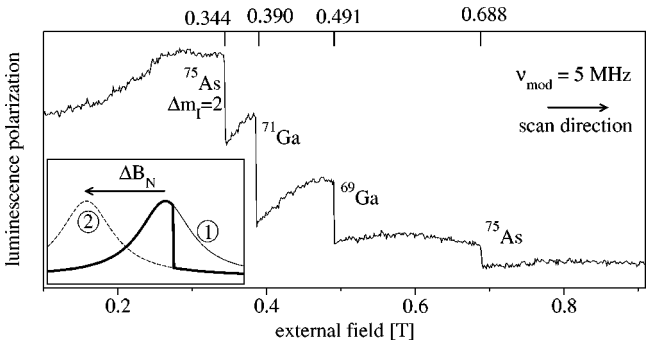

FIG. 3. All-optical NMR-spectrum at a fixed modulation frequency of 5 MHz using intensity modulation of the laser and scanning the external field from 0.1 to 0.9 T. Three of the four transitions can be associated with $\Delta m_I = \pm 1$ transitions of the three relevant nuclei; the fourth represents an ^{75}As $\Delta m_I = \pm 2$ transition. The inset indicates how the sudden change in the luminescence polarization at the NMR resonance frequency can be understood as a shift of the underlying Hanle curve: when the resonance condition is fulfilled, the nuclear spins are saturated and the corresponding nuclear field vanishes.

electro-optical modulator (EOM) and a polarizer. A quarter-wave plate created circularly polarized light, and the beam was focused to a spot size of approximately 100 μm in diameter.

We used an oblique Hanle setup for optical detection of the NMR transitions, with an angle of 73° between the surface-normal of the sample and the external magnetic field.[13,14] The laser was incident along the surface normal. The photoluminescence was focused onto the entrance slit of a 1 m Czerny-turner monochromator (spectral resolution 0.04 nm) to suppress scattered laser light and to select the photoluminescence from the 19.7 nm quantum well. The light was detected by an avalanche photodiode with a bandwidth of 100 kHz.

Polarization measurements of the photoluminescence were performed with a 50 kHz photoelastic modulator (PEM) and a polarizer. A lock-in detector referenced to the PEM extracted the difference between circular polarization intensities. The degree of polarization was obtained by normalizing the lock-in signal to the average intensity. The modulation frequency of the laser beam was of the order of a few MHz, much higher than the frequency of the PEM, and too high to be detected by the photodetector.

III. ALL-OPTICAL SPECTRA

A. Overview

In the oblique Hanle geometry, the hyperfine interaction between the polarized nuclear and electron spin system, when treated as an averaged system, can be regarded as an additional, effective magnetic field acting on the electron spins. The strength of this nuclear field can be determined by a Hanle measurement. Figure 2 shows the polarization of the photoluminescence, measured with circularly polarized excitation as a function of the magnetic field strength (a displaced Hanle curve). The peak of the polarization curve indicates that at this value, the external field is equal in strength and opposite in orientation to the effective nuclear field. Correspondingly, the total magnetic field acting on the electron spins vanishes and the polarization of the luminescence reaches a maximum.

The curve presented in Fig. 2 was measured after pumping the sample for 5 min in an external field of 1.5 T and subsequently scanning the field from 1.5 to 0 T within 20 sec. The width of the curve (HWHH) is of the order of 0.4 T, significantly larger than that of the unshifted Hanle curve (not shown), where the width was $\Delta B = 0.13$ T. The zero-field polarization of the unshifted Hanle curve was $P_0 = 0.29$, corresponding to an exciton recombination time τ_{rec} of 0.76 ns, and a spin lifetime τ_S of 0.31 ns. For the displaced Hanle curve, the peak polarization decreased to 0.2 and the line shape changed from Lorentzian to roughly Gaussian. This broadening is largely due to the nonequilibrium situation, averaged over the beam profile of the pump laser beam.

Initial all-optical NMR experiments were performed by scanning the magnetic field while modulating the laser intensity at a constant frequency of $\nu_{mod} = 5$ MHz. Figure 3 shows an example of such a scan covering the range from 0.1 to 0.9 T. At four distinct field values, the luminescence polarization shows sudden drops. As explained in Fig. 3, the shape of this spectrum can be understood as arising from sudden shifts of the Hanle curve when the resonance condition is matched for one of the nuclear spin species.

Three of these features correspond to the field positions expected for the resonances of the three nuclear spin species contained in GaAs (^{75}As, ^{69}Ga, ^{71}Ga). The drop at 0.344 T occurs at half the field value of the ^{75}As transition. It can be identified with a $\Delta m_I = \pm 2$ transition of the ^{75}As nucleus ($m_I = -3/2 \leftrightarrow +1/2$; $m_I = -1/2 \leftrightarrow +3/2$), as discussed in detail below.

B. High resolution spectra

The individual transitions can be measured at higher resolution by keeping the field fixed and scanning the frequency over the resonance lines. Figure 4 indicates how the NMR transitions are observed under these conditions: initially, the nuclear field is stronger than the external field. As the scanning modulation frequency reaches the resonance condition, the nuclear spins are saturated and the nuclear field is dimin-

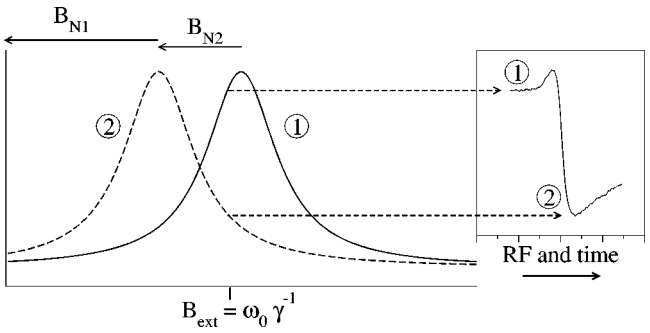

FIG. 4. Shift of the Hanle curve during a scan through resonance at fixed external magnetic field. At the beginning of the scan the Hanle curve (position 1) is shifted by the effective nuclear field $B_{N1}+B_{N2}$ from all isotopes. When the modulation frequency reaches the resonance condition, saturation of one nuclear spin species reduces B_{N2} to zero, thereby shifting the Hanle curve to position 2. The observed polarization, which is shown in the inset, passes through a maximum when $B_{N1}+B_{N2}+B_{\rm ext}=0$, decreases to the value determined by the second Hanle curve, and increases again due to optical pumping when the modulation frequency is far from resonance.

ished. The Hanle curve correspondingly shifts to lower field values. As its maximum passes through the current field setting, the luminescence polarization reaches a maximum and subsequently decreases.

Figure 5 summarizes the resulting spectra for the three isotopes. Parts (a)–(c) represent the $\Delta m_I=\pm 1$ transitions, while parts (d)–(f) represent the $\Delta m_I=\pm 2$ transitions. The resonance frequency for all transition can be written as

$$\omega_{\rm mod}=\gamma_n B_0|\Delta m_I|. \tag{1}$$

Each spectrum shows the experimental data (dots), a fitted spectrum (line), and the corresponding NMR absorption spectrum (inset), which was calculated from the fitting parameters by removing the convolution by the Hanle curve. We deconvoluted the signals with the unshifted, as well as with the shifted Hanle curve. The parameters of interest here were not influenced by the type of deconvolution, resulting in identical NMR spectra for both types of data analysis. For the spectra displayed in this paper, we consistently used the parameters of the unshifted Hanle curve. For the shape of the NMR lines, we found better agreement with a Gaussian line shape than with a Lorentzian.

The ^{75}As, $\Delta m_I=\pm 1$ spectrum [see Fig. 5(a)] contains three well-resolved resonances. They can be identified with the three magnetic dipole transitions of a spin 3/2 with a small quadrupolar splitting. While one expects three degenerate NMR transitions in bulk GaAs, which has cubic symmetry with a T_d $\{\bar{4}3m\}$ crystallographic point group, it is well known that mechanical stress lifts this degeneracy.[15] Under the same conditions, the $\Delta m_I=\pm 2$ spectrum [see Fig. 5(d)] contains only two resonances, which can be identified with the two possible $\Delta m_I=\pm 2$ transitions in a spin-3/2 system. The separation between these two lines ($\Delta\nu=29.6$ kHz) agrees with the separation between the outer

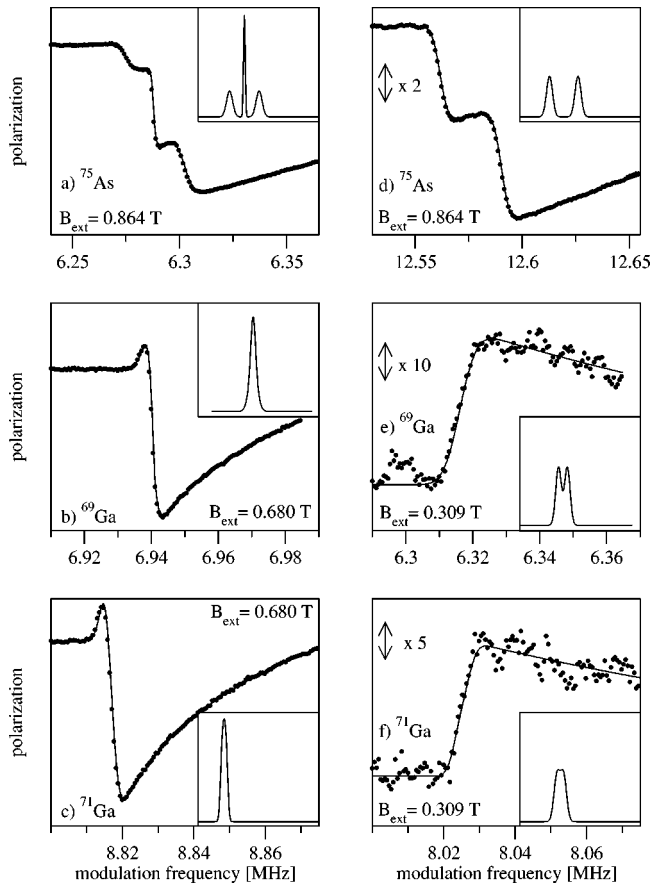

FIG. 5. High-resolution spectra of individual isotopes, measured with intensity modulation at constant magnetic field. (a)–(c) $\Delta m_I=\pm 1$ transitions; (d)–(f) $\Delta m_I=\pm 2$ transitions. Points: experimental data; curve: theoretical fit; inset: NMR spectrum calculated from fit parameters.

lines of the single quantum spectrum ($\Delta\nu=29.6$ kHz). These spectra clearly confirm the assignment of the $\Delta m_I=\pm 2$ transition.

Such two-quantum ($\Delta m_I=2$)-single photon transitions, which should be contrasted to the n-quantum–n-photon transition usually observed in pulsed NMR spectroscopy,[16,17] have been observed in conventional NMR in the context of overtone spectroscopy,[18] by acoustic resonance,[19,20] by electric resonance,[21] and in low-field NMR.[22–24] In the case of low-field NMR, the transitions observed are so-called flip-flip transitions, where two (or more) spins flip simultaneously. Since these transitions are strongly suppressed at higher fields, the observed transitions are some four orders of magnitude stronger than the calculated transition strengths for flip-flip transitions. Furthermore, flip-flip spectra should contain more than two resonance lines. We therefore tentatively assign them to single-spin, two-quantum, single photon transitions, and give additional evidence for this assignment in the subsequent section.

The quadrupolar splitting of the ^{69}Ga and ^{71}Ga resonances is 3.4 and 2.1 kHz, respectively, 4 and 7 times smaller than the ^{75}As splitting. Since the nuclear quadrupole moments for the two gallium isotopes are only two to three times smaller than that of arsenic, we conclude that the dis-

tortion causes different electric field gradients (EFG's) at the two nuclear sites.[12,25]

IV. COUPLING MECHANISMS

A. Magnetic dipole vs electric quadrupole interaction

While the field and frequency scans clearly established that the modulation of the laser beam can induce transitions between the nuclear spins, they do not indicate the mechanism of this process. Two types of interactions are known to be relevant for these spins: magnetic dipole and electric quadrupole couplings.[26] Although the Hanle effect is a clear indication of the magnetic interaction between the nuclear spin system and the electron spins, and the magnitude of the (average) nuclear field acting on the electron spins is easily extracted from the shift of the Hanle curve, there is no quantitative information about the interaction strength acting on the nuclei.

Under our experimental conditions, it is sufficient to discuss the effect of the optical modulation on the nuclear spin system in terms of time dependent perturbation theory. The transition probability between two levels $|a\rangle$ and $|b\rangle$ is then

$$W_{ab}=\frac{2\pi}{\hbar^2}|\langle b|\mathcal{H}_{\rm int}|a\rangle|^2 f(\omega), \tag{2}$$

where $\mathcal{H}_{\rm int}$ represents the coupling Hamiltonian and $f(\omega)$ the spectral density function. The main difference between the magnetic dipole and electric quadrupole interaction is that the magnetic interaction can only induce transitions with $\Delta m_I=\pm 1$, while the selection rule for electric quadrupole interactions is $\Delta m_I=0,\pm 1,\pm 2$.

To distinguish between the two mechanisms, we measured optically induced NMR spectra with two different modulation schemes. In one experiment, the intensity of the pump laser beam was modulated, thereby modulating the magnetic interaction as well as the electric field. In the second experiment, the polarization was modulated, keeping the intensity constant. This modulation scheme keeps the charge density constant but modulates the electron spin polarization and therefore the magnetic interaction with the nuclear spins. If the electric quadrupole interaction is the relevant coupling mechanism, we therefore expect to see transitions only for the intensity modulation, while a magnetic interaction should produce signals for both experiments.

Figure 6 compares spectra obtained with the two modulation schemes. The top trace was measured with constant polarization, modulating the intensity of the laser beam, while the lower trace was taken at constant intensity, modulating the polarization of the laser beam. The mean intensity, the mean polarization, the position on the sample, its orientation and the scan duration were all constant for both measurements to make them comparable. Both spectra contain resonances at the Larmor frequency; the resonance at 0.62 T, which can be associated with the $\Delta m_I=2$ ^{75}As transition, is only excited in the intensity modulation scheme. In these measurements the field scan direction is opposite to the scan direction used in Fig. 3. This enhances the sensitivity for the $\Delta m_I=\pm 2$ transition at 0.62 T. The scan time is significantly

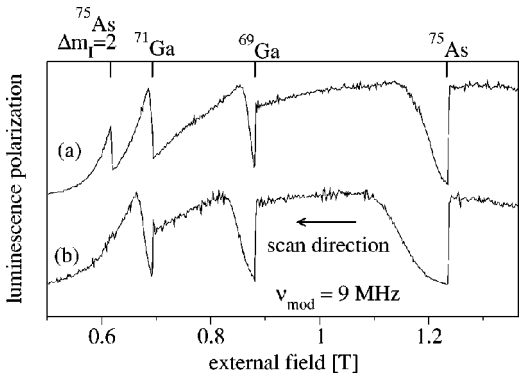

FIG. 6. All-optical NMR spectrum at fixed frequency using (a) intensity modulation and (b) polarization modulation of the laser beam, both with a modulation depth of 0.5, where a full modulation from σ^+ to σ^- is set to a modulation depth of 1.

longer in this measurement, giving the system sufficient time to return to equilibrium between two passages through resonance. During the first three resonance transitions, the maximum of the Hanle curve passes through the current field position, and again (in the opposite direction) during the subsequent repumping period.

These spectra clearly show that both mechanisms are active. For $\Delta m_I=\pm 2$ transitions, where the magnetic dipole mechanism is absent, the electric quadrupole mechanism remains. For $\Delta m_I=\pm 1$ transitions, both interactions contribute. For these transitions, the electric quadrupole interaction can be neglected, as discussed by Kalevich.[5] He compares the NMR-signals by intensity and polarization modulation for $\Delta m_I=\pm 1$ excitation in Bulk GaAs, observing no difference between both modulation schemes. A quantitative analysis for the two mechanisms in the subsequent section provides additional evidence.

B. Magnetic dipole interaction

In close analogy to the effective nuclear field acting on the electron spins, we can model the effect of the hyperfine interaction on the nuclear spins as an alternating magnetic field, for which only the component perpendicular to the static magnetic field is relevant. In the rotating field approximation, the interaction Hamiltonian can then be written as

$$\tilde{\mathcal{H}}_{\rm rf}=\frac{1}{2}\gamma_n\hbar B_1 I_{\pm}. \tag{3}$$

B_1 is the amplitude of the effective rotating magnetic field coupling to the nuclear spin $I_{\pm}$. Since the density of electron spins is much smaller than that of the nuclear spins, this field is many orders of magnitude smaller than the nuclear field acting on the electrons.

To determine the coupling strength, we measured the time dependence of the nuclear spin polarization after switching on the modulation. For a spin $I=3/2$ with resolved quadrupolar splitting, we expect the nuclear spin polarization to decay as

$$I_z(t)=I_{zA}e^{-2W_A t}+I_{zB}e^{-2W_B t}+I_{zC}e^{-2W_C t}, \tag{4}$$

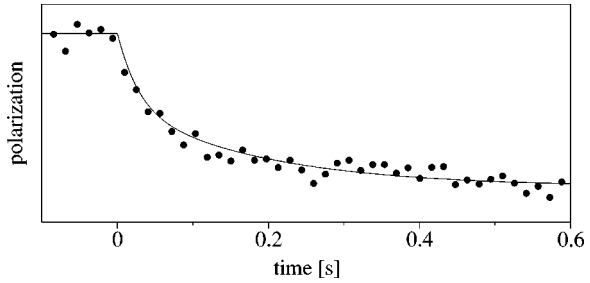

FIG. 7. Time dependence of the photoluminescence polarization during modulation at the ^{75}As $\Delta m_I = 1$ resonance frequency with an amplitude of 200 W cm^{-2}.

where the transition probabilities are, according to Eqs. (2) and (3)

$$W_A = \frac{3}{2}\pi\gamma_n^2 B_1^2 f(\omega - \omega_Q), \tag{5}$$

$$W_B = 2\pi\gamma_n^2 B_1^2 f(\omega), \tag{6}$$

$$W_C = \frac{3}{2}\pi\gamma_n^2 B_1^2 f(\omega + \omega_Q). \tag{7}$$

The index (A, B, C) refers to the three transitions ($+\frac{3}{2} \leftrightarrow +\frac{1}{2}$, $+\frac{1}{2} \leftrightarrow -\frac{1}{2}$, $-\frac{1}{2} \leftrightarrow -\frac{3}{2}$), $f(\omega)$ represents the spectral density function of the relevant transition, and ω_Q the quadrupole splitting. I_{zA}, I_{zB}, and I_{zC} are the polarizations for each transition.

Figure 7 shows a typical example of the observed decay when the modulation was resonant with the ^{75}As transition, together with a fit to the data that includes the dependence of the optical polarization on the nuclear spin polarization. When the modulation amplitude was increased, the observed decay rate of the arsenic polarization increased quadratically with the modulation amplitude (see Fig. 8). According to Eqs. (5)–(7) the transition probability is proportional to the square of B_1. The observed decay is a superposition of the three transitions. Each rate is proportional to $f(\omega)$ of the corresponding transition. The measured transition probabilities and the calculated rotating magnetic field amplitudes are summarized in Table I for an intensity modulation of 100 W cm^{-2}. This quadratic dependence implies a linear increase

TABLE I. Experimental results at $\Delta m_I = \pm 1$.

	γ_n [10^6 s^{-1} T^{-1}]	δ_B [b] [kHz]	W_B [a] [s^{-1}]	B_1 [a] [μT]
^{75}As	45.78±0.03	1.0	6.3±0.4	2.5±0.1
^{69}Ga	64.21±0.04	1.0	7±1	1.9±0.3
^{71}Ga	81.53±0.06	1.5	13±1	2.5±0.1

[a]Mean value at 100 W cm^{-2}.
[b]Half width at half maximum of the transition.

of the effective magnetic field strength with the modulation amplitude (see Fig. 9). This agrees with the prediction of a simple model where the average strength of the hyperfine coupling acting on the nuclear spin system is proportional to the density of the photoexcited electrons.

For the two gallium isotopes, the effective magnetic field also increases linearly at small modulation amplitudes (see Fig. 9). At higher modulations, the dependence becomes weaker. Spin diffusion may be responsible for this nonlinear behavior: Since the polarization process occurs on a time scale of minutes, the nuclear spin polarization established in the vicinity of the trapped excitons is partly transferred to nuclei that do not directly interact with the excitons. In contrast to a rf saturation, the optical saturation is effective only for directly coupled spins; spin diffusion should therefore transport nuclear spin polarization back to the excitons. We expect that a more detailed analysis, which is beyond the scope of this paper, would show contributions on the saturation rate as well as on the rate at which the nuclear spin polarization is reestablished after saturation. Figure 9 indicates that the deviation is significantly stronger for the two Ga isotopes than for ^{75}As. An interpretation of this result might be attempted if the spin diffusion constants for the three isotopes were known. The higher gyromagnetic ratios would favor the Ga isotopes, but the isotopic dilution favors ^{75}As.

C. Electric quadrupole interaction

The $\Delta m_I = \pm 2$ transition couples only to the electric quadrupole interaction. The coupling Hamiltonian for this process can be written as

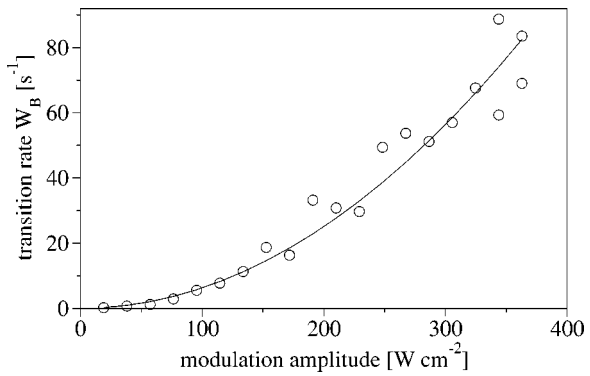

FIG. 8. Dependence of ^{75}As $\Delta m_I = \pm 1$ transition rate on intensity modulation amplitude.

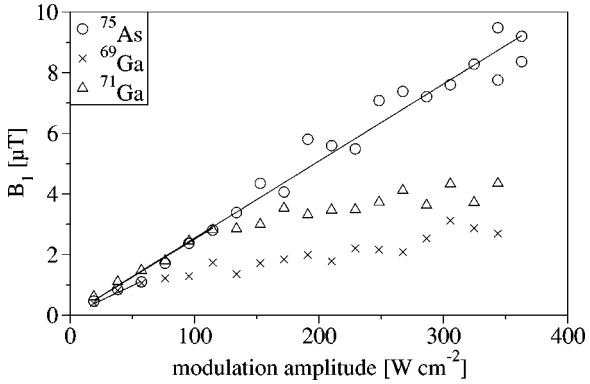

FIG. 9. Effective rf field for ^{75}As and Ga as a function of the intensity modulation amplitude.

$$H_E = \frac{eQ(V_{xx} - V_{yy}) \pm iV_{xy}}{8I(2I-1)} I_{\pm}^2 . \quad (8)$$

To assess the microscopic details of the coupling mechanism, we consider first the change of the EFG at the site of the nucleus due to the presence of an electron. A spherical unit charge with the exciton radius $r = 10$ nm contributes an EFG of -2×10^{14} V m^{-2} in a distance of 10 nm from the center of the exciton.

Since the nuclei in GaAs are located at positions that lack inversion symmetry, there is also an indirect process, which couples the homogeneous electric field to the nuclear quadrupole moment.[25] The matrix element of the induced EFG is[27,12]

$$V_{ij} = (V_{ij})_{E=0} + \sum_k C_{ijk} E_k , \quad (9)$$

$$C_{ijk} = \sum_k R_{ijk} + \sum_k \sum_{lm} S_{ijlm} d_{lmk} , \quad (10)$$

where R_{ijk} describes the generation of an EFG by an applied electric field $\vec{E}$ at constant strain. The second term describes the EFG produced by piezoelectric strain. The coupling constant C_{ijk}, vanishes except where $i \neq j \neq k$ and all these nonzero elements are equal. We combine the indices j,k in the usual Voigt notation to $V_{ij} = V_{ji} = C_{14} E_k$ and $V_{ii} = 0$.

Using the literature data for C_{14} of arsenic[27] and an electric field of 10^6 V m^{-1} due to the presence of the exciton, we estimate a contribution to the EFG of approximately 10^{18} V m^{-2} for the indirect mechanism—significantly more than the direct mechanism. For a $\Delta m_I = \pm 2$ transition, there are only two transitions, and the nuclear spin polarization decays as

$$I_z(t) = I_{zD} e^{-2W_D t} + I_{zE} e^{-2W_E t} \quad (11)$$

with decay rates

$$W_D = \frac{\pi}{24\hbar^2} e^2 Q^2 V_{ij}^2 f(\omega - \omega_Q), \quad (12)$$

$$W_E = \frac{\pi}{24\hbar^2} e^2 Q^2 V_{ij}^2 f(\omega + \omega_Q). \quad (13)$$

The index (D, E) refers to the transitions ($\frac{3}{2} \leftrightarrow -\frac{1}{2}$, $\frac{1}{2} \leftrightarrow -\frac{3}{2}$).

As for the single quantum transitions, we measured the decay rates as a function of the modulation amplitude. The measured rate constants, summarized in Fig. 10, increase quadratically with the modulation amplitude. This result indicates that the EFG is proportional to the density of photoelectrons.

Since the indirect process is significantly larger, we neglect the direct process. Using the coupling constant C_{14} and Eqs. (9), (12), and (13), we estimate the effective alternating electric field E_1 from the transition rates. Table II shows the estimated electric field for a modulation amplitude of 100 W cm^{-2}. Different values have been published for the coupling constants Q and C_{14}.[25,27] As shown in Table II, the variation of these parameters translates into a large uncertainty of the electric field values (a factor of 4).

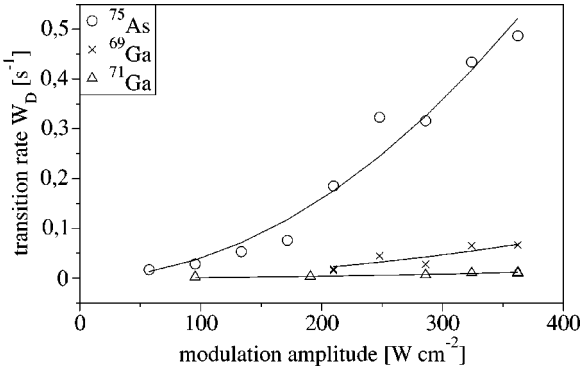

FIG. 10. Dependence of the $\Delta m_I = \pm 2$ transition rate on intensity modulation amplitude for all three isotopes.

Figure 11 shows the dependence of the effective field on the modulation amplitude. The roughly linear increase with a similar gradient for all three isotopes agrees with the assumption that the field is due to photogenerated charges. Since the coupling strength for the electric quadrupole interaction is significantly smaller than that of the magnetic dipole transitions, we conclude that the single quantum transitions are dominated by the magnetic coupling mechanism, as assumed in the evaluation of the data for the single quantum transitions.

V. CONCLUSIONS

The data presented here show clearly that a modulation of a pump laser beam can induce transitions between nuclear

TABLE II. Conversion of pump rates to effective electric field strength. The published data for the coupling constants Q and C_{14} are listed and used to convert the observed transition probability to effective electric fields. We could not find independent measurements of Q and C_{14}; therefore we used these data sets from one measurement. The differences between the values of C_{14} for the two Ga isotopes reflect experimental uncertainties.

	W_D [a] [s^{-1}]	δ_D [e] [kHz]	Q [10^{-29} m^2]	C_{14} [10^{12} m^{-1}]	E_1 [a] [V m^{-1}]
^{75}As	0.040±0.004	2.8	3[b]	1.55[b]	830±40
			2.9[c]	2.93[c]	450±20
			2.9[d]	3.16[d]	420±20
^{69}Ga	0.005±0.002	2.2	2.318[b]	1.05[b]	860±170
			1.9[c]	2.85[c]	390±80
			1.9[d]	2.72[d]	405±80
^{71}Ga	0.0009±0.0001	1.4	1.416[b]	0.9[b]	520±30
			1.2[c]	2.81[c]	200±10
			1.2[d]	2.60[d]	210±10

[a]Mean value at 100 W cm^{-2}.
[b]Values from Gill *et al.* (Ref. 27).
[c]Values from Dumas *et al.* crystal I (Ref. 25).
[d]Crystal II.
[e]Half width at half maximum of the transition.

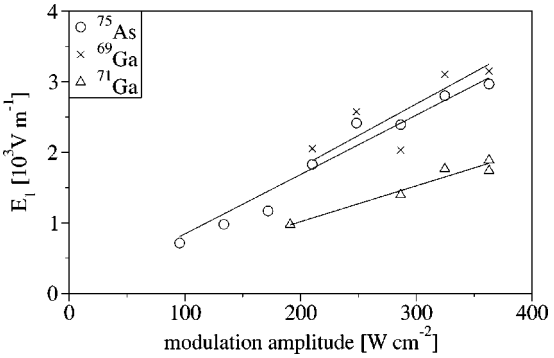

FIG. 11. Variation of associated electric field strength with intensity modulation amplitude.

spin states. For magnetic dipole transitions, the hyperfine interaction is the dominant mechanism for coupling to the nuclear spins. In addition, the charge distribution of photoexcited carriers couples to the nuclear quadrupole moment. For $\Delta m_I = \pm 2$ transitions, this is the dominant coupling mechanism. Kalevich,[5] who reported similar experiments in bulk GaAs, found no evidence for the quadrupole mechanism. This is not surprising, considering that the electric mechanism is significantly weaker and he did not observe the $\Delta m_I = \pm 2$ transitions, where the magnetic dipole mechanism is absent.

Both mechanisms are active when intensity modulation is used. If, instead, the polarization of the laser beam is modulated, at constant intensity, the charge density remains constant. In this case, the electric mechanism is absent, while the magnetic mechanism remains and only dipole transitions are observed. In contrast to the double quantum resonance condition of conventional NMR, where two rf photons induce a double quantum transition, the coupling through the electric quadrupole interaction requires only a single photon, in close analogy to overtone spectroscopy.

To obtain quantitative measurements for the interaction strength, we performed time-dependent measurements of the nuclear spin polarization and extracted the couplings from a rate-equation analysis of these data. Malinowski and Harley[28] have studied the time dependence of the *electron* spin polarization, which occurs on a much shorter time scale; on our experimental time scale, the electron spin system is in equilibrium.

In conclusion, we have shown that a suitable choice of modulation scheme, modulation frequency, and magnetic field strength allows one to excite single quantum $\Delta m_I = \pm 1$ or $\Delta m_I = \pm 2$ transitions by purely optical means. Such experiments may prove advantageous in situations where it is difficult or impossible to apply radio frequency fields to the sample.

ACKNOWLEDGMENTS

We gratefully acknowledge the loan of a sample from Professor Andreas D. Wieck and Dr. Soheyla Eshlaghi. Part of this work was supported by the DFG through the Graduiertenkolleg Festkörperspektroskopie.

*Current address: TOPTICA Photonics AG, Fraunhoferstrasse 14, 82152 Martinsried, Germany.

[1] S. E. Barrett, R. Tycko, L. N. Pfeiffer, and K. W. West, Phys. Rev. Lett. **72**, 1368 (1994).
[2] D. Paget, G. Lampel, B. Sapoval, and V. I. Safarov, Phys. Rev. B **15**, 5780 (1977).
[3] V. K. Kalevich, V. D. Kul'kov, and V. G. Fleisher, Sov. Phys. Solid State **22**, 703 (1980).
[4] V. K. Kalevich, V. D. Kul'kov, and V. G. Fleisher, Sov. Phys. Solid State **23**, 892 (1981).
[5] V. Kalevich, Sov. Phys. Solid State **28**, 1947 (1986).
[6] J. M. Kikkawa and D. D. Awschalom, Science **287**, 473 (2000).
[7] G. Salis, D. T. Fuchs, J. M. Kikkawa, D. D. Awschalom, Y. Ohno, and H. Ohno, Phys. Rev. Lett. **86**, 2677 (2001).
[8] W. E. Bell and A. L. Bloom, Phys. Rev. Lett. **6**, 280 (1961).
[9] Y. Fukuda, J. Hayashi, K. Kondo, and T. Hashi, Opt. Commun. **38**, 357 (1981).
[10] H. Harde, H. Burggraf, J. Mlynek, and W. Lange, Opt. Lett. **6**, 290 (1981).
[11] H. Klepel and D. Suter, Opt. Commun. **90**, 46 (1992).
[12] J. G. Kempf and D. P. Weitekamp, J. Vac. Sci. Technol. B **18**, 2255 (2000).
[13] M. I. Dyakonov, V. I. Perel, V. L. Berkovits, and V. I. Safarov, Sov. Phys. JETP **40**, 950 (1975).
[14] B. P. Zakharchenya, V. K. Kalevich, V. D. Kulkov, and V. G. Fleisher, Sov. Phys. Solid State **23**, 810 (1981).
[15] V. L. Bogdanov and V. V. Lemanov, Sov. Phys. Solid State **10**, 159 (1968).
[16] J. Baum, M. Munowitz, A. N. Garroway, and A. Pines, J. Chem. Phys. **83**, 2015 (1985).
[17] J. Baum, K. K. Gleason, A. Pines, A. N. Garroway, and J. A. Reimer, Phys. Rev. Lett. **56**, 1377 (1986).
[18] R. Tycko and S. J. Opella, J. Am. Chem. Soc. **108**, 3531 (1986).
[19] M. Menes and D. I. Bolef, Phys. Rev. **109**, 218 (1958).
[20] W. G. Proctor and W. Robinson, Phys. Rev. **104**, 1344 (1956).
[21] I. I. Sadykov and E. P. Khaimovich, JETP Lett. **34**, 419 (1981).
[22] J. R. Franz and C. P. Slichter, Phys. Rev. **148**, 287 (1966).
[23] V. K. Kalevich, V. D. Kulkov, I. A. Merkulov, and V. G. Fleisher, Sov. Phys. Solid State **24**, 1195 (1982).
[24] V. K. Kalevich and V. G. Fleisher, Bull. Acad. Sci. USSR, Phys. Ser. (Engl. Transl.) **47**, 5 (1983).
[25] K. A. Dumas, J. F. Soest, A. Sher, and E. M. Swiggard, Phys. Rev. B **20**, 4406 (1979).
[26] A. Abragam, in *Principles of Nuclear Magnetism* (Oxford Science Publications, Oxford, 1994).
[27] D. Gill and N. Bloembergen, Phys. Rev. **129**, 2398 (1963).
[28] A. Malinowski and R. T. Harley, Solid State Commun. **114**, 419 (2000).